Scripta Materialia 148 (2018) 20–23

Contents lists available at ScienceDirect

Scripta Materialia

journal homepage: www.elsevier.com/locate/scriptamat

Regular article

Amorphous alloy strengthened stainless steel manufactured by selective laser melting: Enhanced strength and improved corrosion resistance

Yuanjie Zhang, Jinliang Zhang, Qian Yan, Lei Zhang, Min Wang, Bo Song *, Yusheng Shi

School of Material Science and Engineering, State Key Laboratory of Materials Processing, Die & Mould Technology, Huazhong University of Science and Technology, Wuhan 430074, China

ARTICLE INFO

Article history:
Received 12 December 2017
Received in revised form 12 January 2018
Accepted 12 January 2018
Available online xxxx

Keywords:
Selective laser melting
Amorphous alloys
Stainless steel
Mechanical properties

ABSTRACT

In order to enhance the strength and wear characteristics of stainless steel, Fe-based amorphous alloy with ultra-high strength was introduced to reinforce stainless steel through selective laser melting. The intrigued finding was that the amorphous alloy strengthened stainless steel exhibited an increased tensile strength from 819 MPa to 1090 MPa, a lower coefficient of friction (from 0.62 to 0.49) and a higher corrosion resistance. The enhancements of properties are contributed to the oxygen purification of Y element and solid solution of Co and Mo elements, as well as the grain refinement strengthen with the introduction of the amorphous alloy.

Austenitic stainless steel alloys have been widely used in aerospace and biomedical domains [1]. Nevertheless, their low hardness and poor wear characteristics have weakened reliability and limited their extensive applications [2–3]. Previous researches have concentrated on the coating [4–6], nitriding [7–9] and carburization [10–12] to increase the performance of austenitic stainless steel by modifying hardness and wear resistance of the surface. Such reinforcement only occurs on the surface of stainless steel, how to strengthen the core material thus becomes a crucial issue.

Efforts have been devoted to fabricate stainless steel composites in recent years by dispersing ceramic phases in the stainless steel matrix. The forming techniques mainly focus on the casting and powder metallurgy [13–15]. These processes are complicate and time consuming, where the expensive molds are usually required and usually results in an undesirable coarse grain structure and heterogeneous composition distribution. By comparison with these traditional techniques, selective laser melting (SLM), as a promising additive manufacturing (AM) technique, exhibits alluring prospects in component fabrication [16–17]. SLM not only shortens the processing cycle and reduce the costs, but also exhibits high design flexibility and produces parts with superior performance [18–19].

Several reinforcements such as TiC [20–21], TiB_2 [22–23], hydroxyapatite (HA) [24], SiC [25], have been used to develop stainless steel matrix composites. AlMangour et al. [22–23] have also investigated the TiB_2/316L stainless steel composites, where the TiB_2 particles homogeneously dispersed and formed nanoscale ring-like structures along the grain boundaries, resulting in enhanced comprehensive stress with increasing contents of TiB_2 particles. Hao et al. [24] have investigated the effect of SLM parameters on 316L stainless steel/hydroxyapatite composite used as load-bearing and bioactive implants. Song et al. [25] have fabricated fully dense nano/submicro-sized carbides reinforced iron matrix composites, which exhibited a higher tensile strength than that of the pure iron. Nevertheless, the poor wettability between ceramic reinforcement (new phase) and stainless steel as well as the residual oxygen inevitably causes defects such as pores at the interface [20], which greatly weakens the performance of the manufactured parts.

Considering that amorphous alloys possesses high strength (such as 3–5 GPa for Fe-based amorphous alloys), hardness and wear resistance due to their isotropic amorphous structure [26–27], it has been prepared induced as coating by laser melting [28]. Cu-based metallic glass has been cladding and remelting to Ti substrates by JTM De Hosson, it reveals hardnesses up to 13 GPa over the full depth of a coating, which are comparable with bulk metallic glass melt–spun ribbons [29]. JTM De Hosson et al. have also deposited porous glass forming alloy powder on mild steel substrates by laser cladding, thus formed a 100 to 500 nm interdendritic austenitic phase and a dendritic dual-phase of ferrite/martensite. The layers have a good wear resistance caused by the growth and accumulation of thick oxide layers comprising nano-scale oxidized wear debris [30]. These indicate that the metallic glasses exhibit excellent wettability with metal substrate and actually increase the surface properties of metal.

The amorphous alloy FeCoCrMoCBY, which has good mechanical properties like high hardness and wear resistance, was added in 316L stainless steel matrix and the composite was prepared by SLM. In this ingredient, the yttrium can actively oxidize with oxygen, purifying the

* Corresponding author.
E-mail address: bosong@hust.edu.cn (B. Song).

https://doi.org/10.1016/j.scriptamat.2018.01.016
1359-6462/

parts in SLM processing and the other contents such as Mo, Cr, and Co have potential to increase corrosion resistance, hardness and wear resistance. Therefore, it is worthy studying whether amorphous alloys can enhance the mechanical properties of stainless steel and what are the reinforcement mechanisms. The microstructural evolution, mechanical properties and corrosion resistance of the SLM-processed amorphous alloy-reinforced 316L stainless steel, were investigated systemically in this work.

The original powders used in this work is commercially pure gas-atomized AISI 316L stainless steel powder (D50 = 43.4 μm) and $Fe_{43.7}Co_{7.3}Cr_{14.7}Mo_{12.6}C_{15.5}B_{4.3}Y_{1.9}$ (at.%) powder (D50 = 13.6 μm). The stainless steel and Fe-based amorphous alloy powders with a mass ratio of 90 to 10 were blended.

All parts were fabricated by EOS M280 SLM machine and protected by argon gas. The experimental parameters adopted in this work are as follows, P = 285 W, scanning speed V = 960 mm/s, powder bed layer thickness h = 40 μm, scan spacing t = 110 μm and scanning direction rotated by 67° alternately among layers.

The microstructure was characterized by field emission scanning electron microscope (SEM, Quanta 650) and transmission electron microscope (TEM, Tecnai G2 F30). The residual stress was detected by X-ray residual stress method (Proto-LXRD). Tensile tests were performed at room temperature with a strain rate of $8.3 \times 10^{-4}\ s^{-1}$, using a Zwick/Roell 020 universal testing machine. The wear experiments were carried out on the SLM printed composite surfaces by ball-on-flat reciprocating tests on a Bruker UMT-2 Tribometer with a Si_3N_4 pin (diameter of 6.35 mm). A sliding distance of 10 mm with sliding speed of 10 mm/s, load of 60 N and a total back-and-forth sliding duration of 60 min have been set for each test at ambient temperature under dry condition. The aggressive medium used in potentiodynamic polarization measurements was 3.5 wt% NaCl solution. The potentiodynamic polarization test was performed using a scan rate of 0.5 mV/s from −0.3 V to +1.3 $V_{Ag/AgCl}$. All tests were repeated 3 times for each condition.

Fig. 1(a) illustrates the SEM original top surface morphology of SLM-processed Fe-based amorphous alloy strengthened stainless steel composite. It is worth noting that some light gray precipitates form and seem to be distributed along the melting pools of the powder bed layer. The corresponding element analysis described in the inset of Fig. 1(a) indicates that the content amount of elements Y and O reaches up to 70 at.% in the strip zones. This is due to that yttrium reactions with oxygen firstly as the amorphous alloy melts during the SLM process. Since yttrium has very strong deoxygenation capacity, yttrium oxide formed during process, then the low-gravity oxide (5.01 g/cm^3) was push aside, distributing along the melting pools. When the next layer melt, the yttrium oxide come-up to the surface, leading to an accumulation yttrium oxide in the original top surface. After the process repeated layer by layer, all the oxide floated to the surface of the parts as shown in Fig. 1(a), while there is no more oxide in other areas. Fig. 1(b) displays the SEM top-view morphology of the composite after polish and the corresponding EDX mapping and element analysis in the inset image indicate that no Y element distribute in the top-view of the specimen while other elements have an even distribution in the top-view. In SLM process, the presence of oxygen leads to the oxidation of the metal, reducing the performance of the SLMed parts. While oxygen sources are always from the original powders and the protective atmosphere, which it is inevitable for current SLM technology. In this work, it found that oxygen can be extracted with the help of Y elements to produce low density oxides and float to the surface of metal parts. It concludes that addition of appropriate elements can realize the purification of impurities in metal materials during SLM process. Fig. 1 (c) and (d) are TEM image and the corresponding diffractional lattice of the composite, respectively. It is confirmed that the corresponding SAD patterns is γ-Fe, and the amorphous can't be detected, which proved that the amorphous has been reaction with 316L stainless steel and Y, Co, Mo elements from the amorphous has been solid solution to matrix.

In order to study the elimination mechanism of the composite after addition of amorphous, the residual stress has been detected on the several points in origin top surface. During SLM processing, the overlapping and central regions of melting pool display different residual stress. So the residual stress of composite ranges from −18.8 to 111.6 MPa, compared with that of 316L stainless steel (from −46.6 to 111.6 MPa). It was reported that the tensile residual stress often appeared in the overlapping region between two adjacent laser scanning passes [31–33].

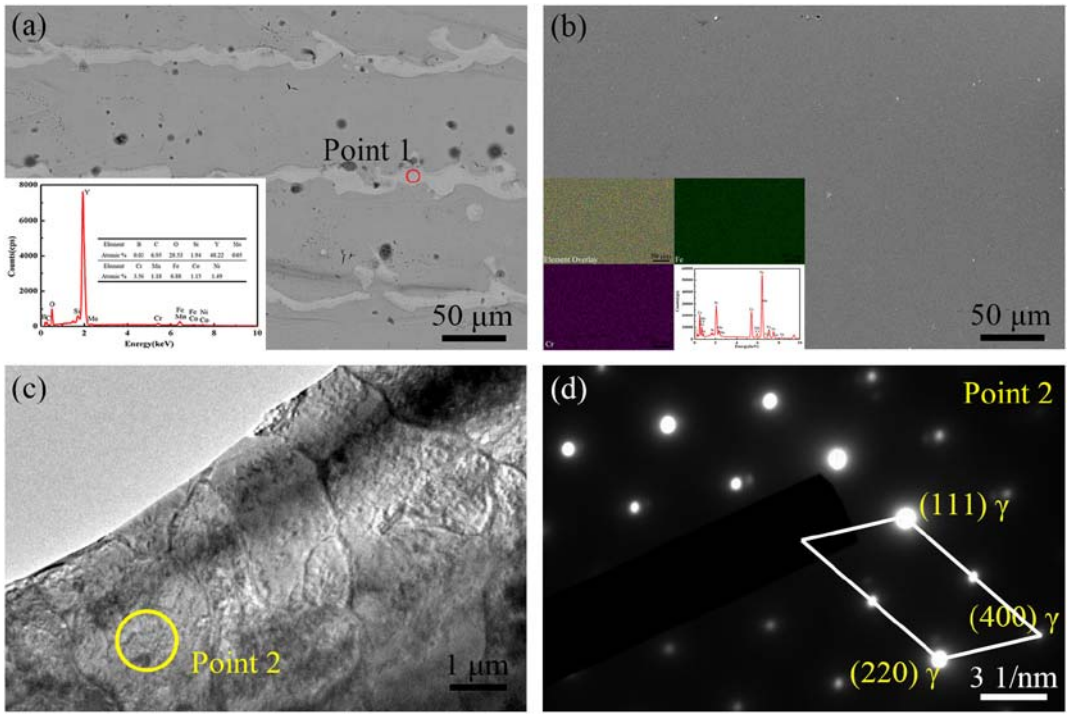

Fig. 1. (a) SEM original top surface and (b) top-view micrograph of composite; (c) (d) TEM image.